



# CHORUS

This is the accepted manuscript made available via CHORUS. The article has been published as:

## Exact Potential Driving the Electron Dynamics in Enhanced Ionization of $H_{2}^{+}$

Elham Khosravi, Ali Abedi, and Neepa T. Maitra

Phys. Rev. Lett. **115**, 263002 — Published 29 December 2015

DOI: [10.1103/PhysRevLett.115.263002](https://doi.org/10.1103/PhysRevLett.115.263002)

# The Exact Potential Driving the Electron Dynamics in Enhanced Ionization of $H_2^+$

Elham Khosravi,<sup>1,2,\*</sup> Ali Abedi,<sup>1,2,†</sup> and Neepa T. Maitra<sup>1,‡</sup>

<sup>1</sup>Department of Physics and Astronomy, Hunter College and the Graduate Center of the City University of New York, 695 Park Avenue, New York, New York 10065, USA

<sup>2</sup>Nano-Bio Spectroscopy Group and European Theoretical Spectroscopy Facility (ETSF), Universidad del País Vasco CFM CSIC-UPV/EHU-MPC and DIPC, Av. Tolosa 72, 20018 San Sebastián, Spain

(Dated: October 19, 2015)

It was recently shown that the exact factorization of the electron-nuclear wavefunction allows the construction of a Schrödinger equation for the electronic system, in which the potential contains exactly the effect of coupling to the nuclear degrees of freedom and any external fields. Here we study the exact potential acting on the electron in charge-resonance enhanced ionization in a model one-dimensional  $H_2^+$  molecule. We show there can be significant differences between the exact potential and that used in the traditional quasistatic analyses, arising from non-adiabatic coupling to the nuclear system, and that these are crucial to include for accurate simulations of time-resolved ionization dynamics and predictions of the ionization yield.

Ionization is a fundamental process in strong-field physics, lying at the heart of many fascinating phenomena such as high harmonic generation, Coulomb explosion, and molecular orbital tomography. The ionization rate (IR) from a molecule can be several orders of magnitude higher than the rate from the constituent atoms at a critical range of internuclear separations. This phenomenon, termed charge-resonance enhanced ionization (CREI), was theoretically predicted [1–4] and verified experimentally [5–7]. The IR enhancement has been explained by a quasistatic argument [2, 4, 8–11], treating the nuclei as instantaneously-fixed point particles, with the electrons following the combined potential from the laser field and the electrostatic attraction to the nuclei. In any experiment however, the nuclei are neither frozen, nor are they point particles; instead their motion can be *strongly* coupled to the electron dynamics and accounting for the coupled electron-ion quantum dynamics can be essential [12]. Further, the electron does not simply follow the field adiabatically, revealed by the multiple subcycle ionization bursts [13, 14]. Calculations treating the full quantum dynamics of the nuclei and electron in  $H_2^+$  [4, 8], and a few experiments, have verified that the essential CREI phenomenon remains robust, although ionic dynamics alter the details. For example, nuclear motion washes out the two-peak structure predicted in the frozen-nuclei analysis [2] into a single broad peak [5]. Further, CREI is subdued if, during the experiment, only little of the nuclear density reaches the critical internuclear separation [15]. Hence, to properly understand, model, and predict the experiment, a fully time-dependent (TD) picture of coupled electronic and ionic motion is needed.

Here, we utilize the exact factorization approach [16–29] to investigate the electron dynamics during CREI. In particular, we study the exact TD potential that drives the electron, introduced by the exact factorization in its reverse form [20], which fully accounts for coupling to both the field and the dynamical nuclei. This exact po-

tential can be remarkably different from the quasistatic potential ( $\epsilon^{\text{qs}}$ ), or even from modifying  $\epsilon^{\text{qs}}$  to account for the width and splitting of the nuclear wavepacket. Therefore dynamical electron-nuclear correlation effects must be included in the calculation. Further, we identify a measure of ionization for fully dynamical studies indicating the regions of the nuclear wavepacket associated with the ionizing electron.

Restricting the motion of the nuclei and the electron in the  $H_2^+$  molecule to the polarization direction of the laser field, the problem can be modeled with a one-dimensional Hamiltonian featuring “soft-Coulomb” interactions [30] (atomic units are used throughout the article, unless otherwise noted):

$$\hat{H}(t) = -\frac{1}{2\mu_e} \frac{\partial^2}{\partial z^2} - \frac{1}{M} \frac{\partial^2}{\partial R^2} - \frac{1}{\sqrt{1 + (z - R/2)^2}} - \frac{1}{\sqrt{1 + (z + R/2)^2}} + \frac{1}{\sqrt{0.03 + R^2}} + \hat{V}_l(z, t) \quad (1)$$

where  $R$  and  $z$  are the internuclear distance and the electronic coordinate as measured from the nuclear center-of-mass, respectively.  $M$  denotes the proton mass while  $\mu_e = (2M)/(2M+1)$  is the electronic reduced mass. The laser field is  $\hat{V}_l(z, t) = q_e z E(t)$  within the dipole approximation where  $E(t)$  denotes the electric field amplitude and  $q_e = (2M+2)/(2M+1)$ . Such a model captures much of the physics of CREI, however it cannot capture all the strong-field molecular phenomena, e.g. rotations that couple strongly via light-induced conical intersections [31].

First we study the dynamics of the system subject to a 50-cycle pulse of wavelength  $\lambda = 800$  nm and intensity  $I = 2 \times 10^{14}$  W/cm<sup>2</sup>, with a sine-squared pulse envelope. Choosing the ground-state as the initial state, we first solve the TD Schrödinger equation (TDSE) numerically exactly. The upper panel of Figure 1, shows the dissociation and ionization probability (IP) and the average internuclear distance versus number of optical cy-

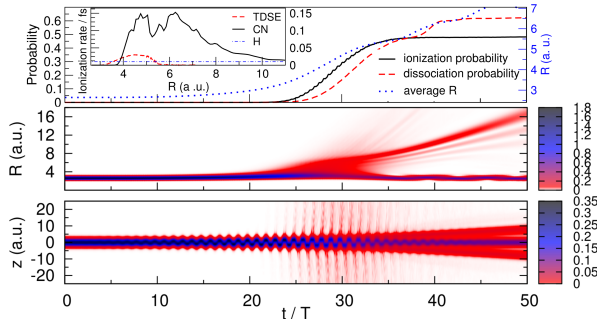


FIG. 1. Top: Average internuclear distance, ionization and dissociation probability versus number of cycles  $t/T$ . The inset depicts the IR for: clamped-nuclei (CN) calculation versus  $R$  (black dashed line), the full TDSE versus  $\langle R \rangle$  (red full line), and the H atom (dash dotted line). Middle (Bottom): contour plot of the TD nuclear (electronic) density.

cles ( $t/T$ ). (The laser period is  $T = 2.67$  fs). Ionization is rapidly onset as we approach the middle of the pulse, slowing down later while the field decreases. The nuclei dissociate primarily via Coulomb explosion following ionization. Most of the ionization occurs when the average internuclear separation  $\langle R \rangle$  is between 4–5 a.u. The inset of the upper panel shows the IR versus  $\langle R \rangle(t)$  (fixed  $R$ ) for fully dynamical (clamped-nuclei) calculation. For clamped-nuclei, the peak near 6.5 a.u. is usually identified with CREI while that near 5 a.u. is associated with symmetry-breaking electron localization [2]. The exact IR, however, has a single broad peak centered between 4 a.u. and 5 a.u. and is smaller than that of the clamped-nuclei calculations, but still higher than the atomic rate, similar to the observations in Refs. [4, 5].

The nuclear charge distribution (middle panel of Figure 1) bifurcates; a large fragment of the nuclear density remains localized, oscillating around the equilibrium separation, while another part begins to dissociate, soon after the ionization is onset, c.f. the electronic density plotted in the lower panel. Therefore considering IR simply versus  $\langle R \rangle$  does not properly indicate the internuclear separations at which the IR is enhanced. A dynamical picture of CREI accounting for coupling to the nuclear distribution as it changes in time is desirable.

Such a picture is provided within the exact factorization framework [16, 17]: in its *reverse* formulation [20], the electron-nuclear wavefunction  $\Psi(\underline{\mathbf{r}}, \underline{\mathbf{R}}, t)$  that solves the full electron-nuclear TDSE can be exactly written as a product  $\Psi(\underline{\mathbf{r}}, \underline{\mathbf{R}}, t) = \Phi(\underline{\mathbf{r}}, t)\chi_{\underline{\mathbf{r}}}(\underline{\mathbf{R}}, t)$ , where  $\Phi(\underline{\mathbf{r}}, t)$  may be interpreted as the electronic wavefunction and  $\chi_{\underline{\mathbf{r}}}(\underline{\mathbf{R}}, t)$  the conditional nuclear wavefunction that parametrically depends on the electronic configuration  $\underline{\mathbf{r}}$  and satisfies the partial normalization condition  $\int d\underline{\mathbf{R}} |\chi_{\underline{\mathbf{r}}}(\underline{\mathbf{R}}, t)|^2 = 1$  for every  $\underline{\mathbf{r}}$  at each  $t$ . The electronic wavefunction yields the exact  $N_e$ -body elec-

tronic density and electronic current-density of the system. The equations that the electronic and nuclear factors satisfy are presented in [20]. The electronic equation, in particular, has the appealing form of a TDSE that contains an exact TD potential energy surface for electrons ( $e$ -TD PES), as well as a TD vector potential: in one-dimension, we can choose a gauge such that the vector potential is zero [16, 17, 20], and then the exact electronic TDSE for our  $\text{H}_2^+$  model reads:

$$\left( -\frac{1}{2\mu} \frac{\partial^2}{\partial z^2} + \epsilon_e(z, t) \right) \Phi(z, t) = i\partial_t \Phi(z, t), \quad (2)$$

where,

$$\epsilon_e(z, t) = \epsilon^{\text{app}}(z, t) + \mathcal{T}_n(z, t) + \mathcal{K}_e^{\text{cond}}(z, t) + \epsilon_e^{\text{gd}}(z, t), \quad (3)$$

is the exact potential driving the electron dynamics. The  $e$ -TD PES,  $\epsilon_e(z, t)$  can be compared with the traditional potentials used to study electronic dynamics, and consists of four terms. First,  $\epsilon^{\text{app}}(z, t) = \langle \chi_z(R, t) | \hat{W}_{en}(z, R) + \hat{W}_{nn}(R) | \chi_z(R, t) \rangle_R + \hat{V}^l(z, t)$  is an approximate potential generalizing the traditional  $\epsilon^{\text{qs}}$  to the case of a quantum nuclear wavepacket [32]. The second term,  $\mathcal{T}_n(z, t) = -\langle \chi_z(R, t) | \partial_R^2 | \chi_z(R, t) \rangle_R / M$ , represents a nuclear-kinetic contribution to the electronic potential from the conditional nuclear wavefunction, while  $\mathcal{K}_e^{\text{cond}}(z, t) = \langle \partial_z \chi_z(R, t) | \partial_z \chi_z(R, t) \rangle_R / \mu$ , is an electronic-kinetic-like contribution from the conditional nuclear wavefunction. Finally  $\epsilon_e^{\text{gd}}(z, t) = \langle \chi_z(R, t) | -i\partial_t | \chi_z(R, t) \rangle_R$  is the gauge-dependent component of the potential. Note that  $\epsilon^{\text{app}}$  reduces to  $\epsilon^{\text{qs}}$  when the nuclear density is approximated classically as a  $z$ -independent delta-function at  $\bar{R}(t) = \langle R \rangle(t)$ ; i.e.  $\epsilon^{\text{qs}}(z, t | \bar{R}(t)) = \hat{W}_{en}(z, \bar{R}(t)) + \hat{W}_{nn}(\bar{R}(t)) + \hat{V}^l(z, t)$ .

We now investigate the  $e$ -TD PES (Eq. 3) and discuss the impact of its components on the electron dynamics. In particular, we ask how well electron propagation on  $\epsilon^{\text{app}}$  performs: is accounting for the width of the nuclear wavepacket, and its correlation with the electron dynamics via the parametric dependence, enough to capture accurately the full electron dynamics? In Figure 2 the exact  $e$ -TD PES,  $\epsilon_e$  (black solid line), and its four components together with  $\epsilon^{\text{qs}}$  (blue dotted) are plotted on the left-hand side at five different snapshots of time in which the field is at the maximum of the cycle. The exact electron density together with the electron density calculated from propagating the electron on  $\epsilon^{\text{qs}}$  and  $\epsilon^{\text{app}}$  are plotted on the right-hand side. We plot the IPs [33] calculated from propagating the electron on different components of  $e$ -TD PES on the left on Fig. 3.

We have chosen times representative of three different phases of the dynamics (refer to Fig. 1): (1) up to  $t \approx 20T$ , for which the dissociation and IPs are still negligible (Fig. 2.a), (2) the second phase,  $\sim 20T < t < \sim 35T$ , when ionization/dissociation mostly occurs (Fig. 2.b-d), (3) the final phase,  $t > 35T$ , in which the system begins to stabilize (panel (e)).

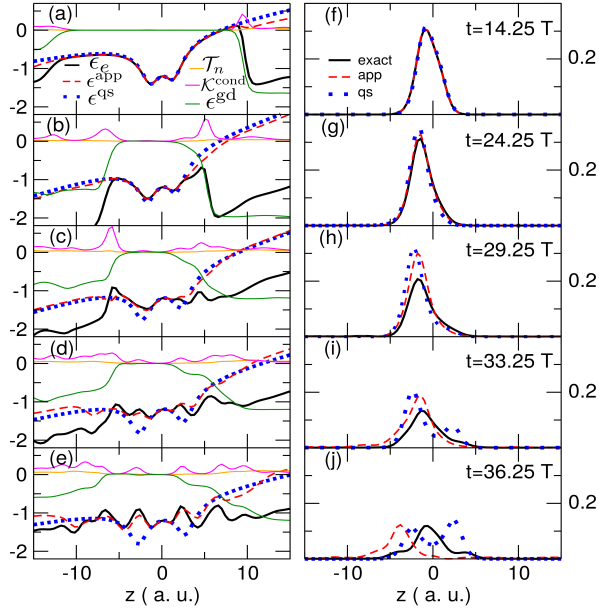


FIG. 2. Left: The exact  $e$ -TDPES  $\epsilon_e$  (black solid line), its various components and  $\epsilon^{\text{qs}}$  (blue dotted line). For very large  $z$ , not shown here, the exact potential is parallel to  $\epsilon^{\text{qs}}$ . Right: The exact electron density together with the electron density calculated from propagating the electron on  $\epsilon^{\text{qs}}$  and  $\epsilon^{\text{app}}$  at different snapshots of time.

During the first phase, the nuclear wavepacket is localized around its initial position and the  $e$ -TDPES,  $\epsilon^{\text{qs}}$ , and approximate potential are essentially on top of each other in the central region ( $|z| < 10$  a.u.), differing only in the tail, where, in particular,  $\epsilon_e$  has a large step downward (Fig. 2.a). The position of the drop corresponds to a sharp change in the  $z$ -dependence of the conditional nuclear wavefunction. Since the density is tiny in the tail region, the overall dynamics is not affected significantly by this feature. In the second phase of the dynamics the nuclear motion begins to pick up, affecting the shape of the exact  $e$ -TDPES in the central region. From this point on the exact potential develops features that are absent in  $\epsilon^{\text{qs}}$  and  $\epsilon^{\text{app}}$ . As part of the nuclear density begins to stretch apart, the  $e$ -TDPES exhibits a double well structure in the up-field side of the potential ( $0 < z < 5$  a.u.), while the down-field side maintains a single well, as evident in panels (b) and (c). Further, the depth of the central wells are decreased compared to  $\epsilon^{\text{qs}}$ . Outside the central region ( $|z| > 5$  a.u.) the  $e$ -TDPES drops down, yielding a barrier that is smaller and narrower than that of  $\epsilon^{\text{qs}}$ . This feature in particular, significantly facilitates the tunnelling ionization of the electron density in the exact dynamics already at  $t = 24.25 T$ , evident in the spreading of the exact density (panel (g), see also left panel of Fig. 3). In the case of the quasistatic and approximate potentials, the ionization is still negligible at this time, due to small tunnelling probability. The dif-

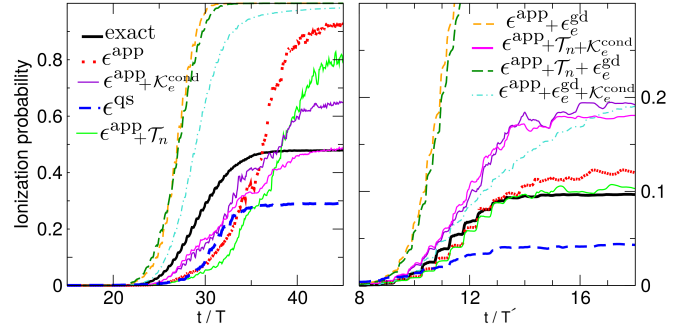


FIG. 3. IPs calculated from propagating the electron on different components of the exact electronic potential as well as on the quasistatic potential. Left:  $\lambda = 800$  nm and  $I = 2 \times 10^{14}$  W/cm<sup>2</sup> (50-cycle). Right:  $\lambda = 600$  nm and  $I = 10^{14}$  W/cm<sup>2</sup> (20-cycle). Legends apply to both.

ferences between the exact  $e$ -TDPES and both  $\epsilon^{\text{app}}$  and  $\epsilon^{\text{qs}}$  continue to grow in the central region ( $|z| < 5$  a.u.) throughout the second phase (panels (b)–(d), and corresponding electronic densities (g)–(i)), as contributions from  $\epsilon_e^{\text{gd}}$  and  $\mathcal{K}_e^{\text{cond}}$  increase and extend closer to the center. It is interesting that  $\epsilon_e^{\text{gd}}$  typically has large steps that lowers the potential on both sides, allowing for more ionization (see also Fig. 3, left panel), while  $\mathcal{K}_e^{\text{cond}}$  develops several (smaller) barrier structures, whose net effect also appears to increase the IP in this phase (see Fig. 3). The  $\mathcal{T}_n$  term has very small barriers in the outer region whose tendency is to confine the density, leading to a decrease in the IP.

By the end of the second phase, at  $t = 33.25 T$  (Fig. 2.d), the exact potential is totally different from  $\epsilon^{\text{qs}}$ , everywhere except for  $|z| < 1$ , presenting a shallow double well structure in both up-field and down-field sides of the potential. Furthermore, the discrepancy between the  $\epsilon^{\text{qs}}$  and  $\epsilon^{\text{app}}$  becomes more noticeable as the nuclear wavepacket splits and dissociates in the field. By this time, there has been significant ionization in all three cases (left panel of Fig. 3), although more in the exact case. Towards the end of the second phase, the IPs of the quasistatic and approximate calculations differ from each other, as expected from the growing discrepancy between their respective potentials.

Entering the third phase of the dynamics (Fig. 2.e), the exact potential differs dramatically from the other two forming four wells in the central region ( $|z| < 6$  a.u.). The two wells in the center are associated with the nuclear density localized around the equilibrium while the other two are associated with the dissociating fragment and move outwards. The  $e$ -TDPES consequently localizes the electronic density in three positions as seen in Fig. 2.j, namely in the center and on each of the dissociating fragments of protons. In the third phase,  $\epsilon^{\text{app}}$  grossly overionizes the system; as  $\epsilon^{\text{app}}$  has many shal-

low barriers and continues to oscillate in the field, failing to stabilize. The  $\epsilon^{\text{qs}}$  retains a deep double well structure throughout the dynamics, in contrast to the exact; toward the end of the pulse the ionization in either of these cases saturates, but the quasistatic fails to get the density and IP correct.

The left panel of Figure 3 shows that neglecting all the electron-nuclear correlation terms except for  $\epsilon^{\text{app}}$  underestimates the ionization at first, but later, as the exact ionization begins to saturate, the ionization from  $\epsilon^{\text{app}}$  continues to grow, and leads ultimately to a significant overestimate of the total ionization. Even propagating on  $\epsilon^{\text{qs}}$ , a crude approximation given the earlier discussion, gives a better IP.

We see from Fig. 3 (left) that adding  $\mathcal{T}_n$  to  $\epsilon^{\text{app}}$  reduces the IP at all times, due to its small confining barriers as mentioned above. On the other hand, adding  $\mathcal{K}^{\text{cond}}$  to  $\epsilon^{\text{app}}$  increases the ionization at first, and then decreases it, giving an overall somewhat improved prediction of the ionization dynamics relative to dynamics on  $\epsilon^{\text{app}}$  alone. Although adding both  $\mathcal{K}^{\text{cond}}$  and  $\mathcal{T}_n$  to  $\epsilon^{\text{app}}$  seems to give a good final IP, the intermediate dynamics is not good. Adding  $\epsilon_e^{\text{gd}}$  to  $\epsilon^{\text{app}}$  drastically overshoots the ionization, yielding ultimately a complete ionization. For the current choice of laser parameters and initial state all these dynamical electron-nuclear correlation terms are important to include to obtain good prediction of the IP. But is this conclusion general? Does  $\epsilon^{\text{app}}$  always perform so poorly?

We performed the same calculations using a 20-cycle pulse of wavelength  $\lambda = 600$  nm and intensity  $I = 10^{14} \text{W/cm}^2$ , with a sine-squared pulse envelope, setting the initial state to be the 6th excited vibrational state (c.f. [4]). The IPs computed from propagating the electron on different components of the exact potential is presented in the right panel of Fig. 3 ( $T' = 2$  fs is the duration of one cycle.). Electron dynamics on  $\epsilon^{\text{app}}$  in this case agrees very well with the exact result that with the addition of  $\mathcal{T}_n$  [34] to  $\epsilon^{\text{app}}$  becomes even better. Other combinations of the potential components do not provide satisfactory results. The quasistatic dynamics underestimates the IP significantly: the exact potential differs substantially from  $\epsilon^{\text{qs}}$  from the start due to the vibrational excitation of the initial state.

It is clear that ionization dynamics depends crucially on coupling to quantum nuclear motion; accounting for both the splitting of the wavepacket as well as its dynamics is important. From which part of the nuclear wavepacket is the ionization mostly occurring? To answer this, we plot a time-resolved,  $R$ -resolved, IP [35] via  $I(R, t) = \int_{z_I} dz |\Psi(z, R, t)|^2$ , with  $\int_{z_I} = \int_{-\infty}^{-z_I} + \int_{z_I}^{\infty}$  and  $z_I = 15$  a.u., in Fig 4 for *both* of the laser parameters studied in this work. In both cases, we observe a clear peak of  $I(R, t)$ , centered around  $6 \text{ a.u.} < R < 7.5 \text{ a.u.}$ , the region predicted by the quasistatic analysis of

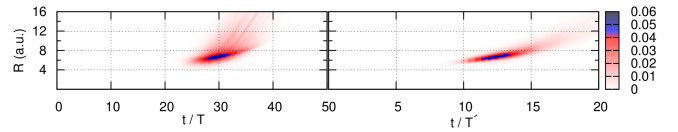


FIG. 4. Time-resolved,  $R$ -resolved IP,  $I(R, t)$ . Left:  $\lambda = 800$  nm and  $I = 2 \times 10^{14} \text{W/cm}^2$  (50-cycle). Right:  $\lambda = 600$  nm and  $I = 10^{14} \text{W/cm}^2$  (20-cycle).

CREI, soon after the fields reach their maximum intensities. Hence, the quantity  $I(R, t)$  represents a very useful measure of CREI in a fully dynamical picture, indicating clearly the dominant internuclear separations at which ionization occurs. This quantity is analogous to the IP at a given internuclear separation in the quasistatic picture (See Supplemental Material.).

In summary, we have found the exact potential driving the electron dynamics in a model one-dimensional  $\text{H}_2^+$  molecule undergoing CREI. The potential provides complete details of the CREI process beyond the quasistatic picture traditionally used to analyze and interpret CREI. The large differences in the two potentials, and the resulting dynamics, reveals the importance of dynamical electron-nuclear correlation terms lacking in previous pictures of CREI: propagating the electrons in a potential that neglects these terms gives large errors in the predictions of the IP. Going beyond the quasistatic treatment by only accounting for the width and splitting of the nuclear wavepacket is generally not enough to get the correct dynamics of CREI. How significant the dynamical electron-nuclear effects are for CREI phenomena in larger systems [36] remains to be investigated. In many-electron systems, the potential is a function of all electronic coordinates. How to accurately model this potential opens a major avenue for future research. One direction is to develop a time-dependent density-functional approach for the coupled systems, that deals with a one-electron Kohn-Sham equation coupled to nuclear degrees of freedom [37]. Another direction would be based on writing an  $N$ -particle wavefunction as a product of  $N$  one-particle functions as proposed in [38]. Future efforts to treat the nuclear dynamics efficiently will explore approximations for the conditional nuclear wavefunction, e.g. stemming from a time-dependent Born-Oppenheimer similar to Ref. [39] but in a reverse formulation. Finally we showed a time-resolved,  $R$ -resolved measure of CREI that accounts for the dynamical electron-nuclear correlation has a clear peak in the region predicted by the quasistatic analysis.

Financial support from the National Science Foundation CHE-1152784 (N.T.M), and Department of Energy, Office of Basic Energy Sciences, Division of Chemical Sciences, Geosciences and Biosciences under Award DE-SC0008623, the European Research Council Advanced

Grant DYNamo (ERC- 2010-AdG-267374) and Grupo Consolidado UPV/EHU del Gobierno Vasco (IT578-13) (E.K, A.A) are gratefully acknowledged.

---

\* elham.etn@gmail.com; Corresponding author

† aliabedik@gmail.com

‡ nmaitra@hunter.cuny.edu

- [1] T. Zuo, S. Chelkowski, and A. D. Bandrauk, *Phys. Rev. A* **48**, 3837 (1993).
- [2] T. Zuo and A. D. Bandrauk, *Phys. Rev. A* **52**, R2511 (1995).
- [3] T. Seideman, M. Y. Ivanov, and P. B. Corkum, *Phys. Rev. Lett.* **75**, 2819 (1995).
- [4] S. Chelkowski, A. Conjusteau, T. Zuo, and A. D. Bandrauk, *Phys. Rev. A* **54**, 3235 (1996).
- [5] I. Ben-Itzhak, P. Q. Wang, A. M. Sayler, K. D. Carnes, M. Leonard, B. D. Esry, A. S. Alnaser, B. Ulrich, X. M. Tong, I. V. Litvinyuk, C. M. Maharjan, P. Ranitovic, T. Osipov, S. Ghimire, Z. Chang, and C. L. Cocke, *Phys. Rev. A* **78**, 063419 (2008).
- [6] E. Constant, H. Stapelfeldt, and P. B. Corkum, *Phys. Rev. Lett.* **76**, 4140 (1996).
- [7] J. Wu, M. Meckel, L. P. H. Schmidt, M. Kunitski, S. Voss, H. Sann, H. Kim, T. Jahnke, A. Czasch, and R. Dörner, *Nature communications* **3**, 1113 (2012).
- [8] S. Chelkowski, C. Foisly, and A. D. Bandrauk, *Phys. Rev. A* **57**, 1176 (1998).
- [9] S. Chelkowski and A. Bandrauk, *J. Phys. B: Atomic, Molecular and Optical Physics* **28**, L723 (1995).
- [10] H. Yu, T. Zuo, and A. D. Bandrauk, *J. Phys. B: Atomic, Molecular and Optical Physics* **31**, 1533 (1998).
- [11] A. D. Bandrauk and F. Légaré, in *Progress in Ultrafast Intense Laser Science VIII* (Springer, 2012) pp. 29–46.
- [12] S. Hammes-Schiffer and A. V. Soudackov, *J. Phys. Chem. B* **112**, 14108 (2008).
- [13] N. Takemoto and A. Becker, *Phys. Rev. Lett.* **105**, 203004 (2010).
- [14] N. Takemoto and A. Becker, *Phys. Rev. A* **84**, 023401 (2011).
- [15] F. Légaré, I. V. Litvinyuk, P. W. Dooley, F. Quéré, A. D. Bandrauk, D. M. Villeneuve, and P. B. Corkum, *Phys. Rev. Lett.* **91**, 093002 (2003).
- [16] A. Abedi, N. T. Maitra, and E. K. U. Gross, *Phys. Rev. Lett.* **105**, 123002 (2010).
- [17] A. Abedi, N. T. Maitra, and E. K. U. Gross, *J. Chem. Phys.* **137**, 22A530 (2012).
- [18] A. Abedi, N. T. Maitra, and E. K. U. Gross, *J. Chem. Phys.* **139**, 087102 (2013).
- [19] A. Abedi, F. Agostini, Y. Suzuki, and E. K. U. Gross, *Phys. Rev. Lett.* **110**, 263001 (2013).
- [20] Y. Suzuki, A. Abedi, N. T. Maitra, K. Yamashita, and E. K. U. Gross, *Phys. Rev. A* **89**, 040501 (2014).
- [21] A. Abedi, F. Agostini, and E. K. U. Gross, *Europhys. Lett.* **106**, 33001 (2014).
- [22] S. K. Min, A. Abedi, K. S. Kim, and E. K. U. Gross, *Phys. Rev. Lett.* **113**, 263004 (2014).
- [23] Y. Suzuki, A. Abedi, N. Maitra, and E. K. U. Gross, *Phys. Chem. Chem. Phys.*, (2015).
- [24] F. Agostini, A. Abedi, Y. Suzuki, S. K. Min, N. T. Maitra, and E. K. U. Gross, *J. Chem. Phys.* **142**, 084303 (2015).
- [25] S. K. Min, F. Agostini, and E. K. U. Gross, *Phys. Rev. Lett.* **115**, 073001 (2015).
- [26] G. Hunter, *International Journal of Quantum Chemistry* **9**, 237 (1975).
- [27] N. I. Gidopoulos and E. K. U. Gross, *Philosophical Transactions of the Royal Society of London A: Mathematical, Physical and Engineering Sciences* **372**, 20130059 (2014).
- [28] L. S. Cederbaum, *J. Chem. Phys.* **138**, 224110 (2013).
- [29] R. Lefebvre, *J. Chem. Phys.* **142**, 074106 (2015).
- [30] J. Javanainen, J. H. Eberly, and Q. Su, *Phys. Rev. A* **38**, 3430 (1988).
- [31] G. J. Halász, Á. Vibók, and L. S. Cederbaum, *J. Chem. Phys.* **6**, 348 (2015).
- [32] Here  $\hat{W}_{en}$  is summation of the third and fourth term of Eq. 1, while  $\hat{W}_{nn}$  is its fifth term.
- [33] Steps in the IP for both cases are associated with the multiple ionization bursts within each optical cycle [13].
- [34] Note that  $\mathcal{T}_n$  is inversely proportional to the nuclear mass, therefore is likely less pronounced for heavier nuclei.
- [35] K. C. Kulander, F. H. Mies, and K. J. Schafer, *Phys. Rev. A* **53**, 2562 (1996).
- [36] I. Bocharova, R. Karimi, E. F. Penka, J.-P. Brichta, P. Lassonde, X. Fu, J.-C. Kieffer, A. D. Bandrauk, I. Litvinyuk, J. Sanderson, *et al.*, *Phys. Rev. Lett.* **107**, 063201 (2011).
- [37] T. Kreibich and E. K. U. Gross, *Phys. Rev. Lett.* **86**, 2984 (2001).
- [38] L. S. Cederbaum, *Chem. Phys.* **457**, 129 (2015).
- [39] L. S. Cederbaum, *J. Chem. Phys.* **128**, 124101 (2008).